Surface-Initiated ATRP of *N*-Isopropylacrylamide from Initiator-Modified Self-Assembled Peptide Nanotubes

J. Couet and M. Biesalski*

Department of Microsystems Engineering (IMTEK), University of Freiburg, Georges-Köhler-Allee 103, 79110 Freiburg, Germany

Received May 29, 2006; Revised Manuscript Received July 28, 2006

ABSTRACT: Peptide−polymer hybrid nanotubes (PPNT) were prepared by a combination of self-assembling functional cyclic peptides and in-situ surface-initiated atom transfer radical polymerization (ATRP). Cyclic peptides that consist of alternating D- and L-amino acids, carrying ATRP initiators in distinct side chains, were self-assembled into hollow nanotubes that expose all initiation moieties at the outer surface, thereby forming a cyclic peptide initiator nanotube (CP-ini). The CP-ini nanotubes were dispersed in 2-propanol, and a surface-initiated ATRP reaction has been performed using *N*-isopropylacrylamide (NIPAM) as monomer, tris[2(dimethylamino)-ethyl]amine (Me_6TREN) as ligand, and additional sacrificial (model) initiator. The molar mass of the resulting PNIPAM can be well controlled by adjusting the polymerization time (i.e., reaction conversion). The solvent-free height of the PNIPAM−PPNT, as measured by statistical analysis of cross sections of atomic force microscopy (AFM) height micrographs, increases with increasing molar mass of the attached PNIPAM chains in a well-controlled manner. The latter allows for the first time to tailor the outer diameter of self-assembled peptide nanotubes in a very precise way without changes to the primary sequence of the peptide ring. The length of the PNIPAM−PPNT remains almost constant with increasing polymerization time; however, at larger polymerization times, a decrease in absolute number of PPNT is observed, and smaller particles are increasingly present due to a breakup of the PNIPAM−PPNT into smaller peptide−polymer hybrid nanoobjects.

Introduction

Channel-forming proteins and peptides are among the most fascinating class of functional nanodevices found in nature. They are responsible for selectively transporting signals in and between cells, which subsequently can initiate a cascade of reactions necessary for cellular function.[1,2] Channels that selectively permit the diffusion of water molecules[3] or small ions,[4] for example, maintain the pressure inside of our cells and are the underlying driving force that cause our muscles to tense. In some cases, nanochannels found in nature even possess interesting properties such as they function as closed reaction chambers[5] or have antibiotic activities.[6]

Driven by the large variety of these different functions natural nanochannels fulfill, scientists are increasingly being attracted to the challenge of designing artificial nanochannels and nanotubes because of possible applications progressing from the use as molecular sieves in advanced separation technologies,[7] the design of nanoscale fluidic transport devices,[8] to the use as ion-selective sensing devices,[9,10] and as novel antibacterial agents.[11] To this, a number of interesting supramolecular design strategies for the preparation of artificial nanochannels have evolved over the past decade, and the state of the art of existing synthetic strategies has been very recently reviewed in detail by Balbo-Block et al.[12]

In contrast to nanotubular materials prepared through templated- or artificial-growth mechanism, supramolecular approaches offer some distinct advantages, such as high convergence in synthesis, regioselective functionalization of interfaces, control of self-assembly, and high yields. Artificial nanotubes can be prepared, for example, by the folding of chainlike molecules into a helical secondary motif.[13,14] The driving forces here are either the precise imprint of geometrical constraints into the primary structure of inherently stiff helices[13] or the thermodynamically controlled folding of molecules into helices that leave an inner void resembling the tubular architecture.[14] Following the design principles of natural channels very closely, Matile and co-workers recently reported the self-assembly of peptide-modified oligo-*p*-phenylenes[16] into a barrel-like architecture that mimics natural channels such as the α-hemolysin.[17] In other examples, artificial nanotubes are prepared by the self-assembly of low-molecular-weight organic molecules, where noncovalent interactions do not only allow for the stacking into a tubular architecture but also modulate the cyclic cross sections along the tubes short axis.[9,15] An interesting work by Percec and co-workers uses dentritic amphiphiles with a dipeptide headgroup that self-assemble into well-defined nanochannels capable of mediating ion transport through a lipid bilayers.[9]

Finally, artificial nanotubes can be prepared by the precise stacking of ring-type molecules.[9] Phenylene,[18] phenylene−ethynylene,[19] and phenylene−diethynylene macrocycles[20] self-assemble into tubular architectures, where the individual rings are held together via $\pi-\pi$-interactions. Interestingly, Höger and co-workers showed that, by modifying the peripheral functions in a precise way, solvent-triggered conformational changes within the backbone of a phenylene−diethynylene macrocycle can switch pore sizes from about 0.4 nm to more than 1 nm.[20]

Following first conceptional work by DeSantis,[21] Ghadiri and co-workers pioneered the design of cyclic peptides that consist of an even number of D- and L-amino acids that can be self-assembled into nanotubular stacks consisting of a large number of peptide subunits by formation of intermolecular hydrogen bonds.[22−24] These cyclic peptides possess a very flat conformation with all amide functions lying perpendicular to the plane of the molecule. The latter allows the buildup of an extended hydrogen-bonded network, preferably in an antiparallel β-sheet fashion.[25] Because of the peptide configuration, all side-chain

* Corresponding author. E-mail: biesalski@imtek.de.

10.1021/ma061200j CCC: $33.50
Published on Web 09/19/2006

functional groups are decorating the outer surface, thereby forming a defined hollow core and allowing simple access for modification of the interfacial chemistry. Similar to the dentritic dipeptides of Percec,[9] cyclic D-/L-peptides are capable of in-situ self-assembling into lipid bilayers, thereby forming an artificial ion channel with transmembrane activities for sodium and potassium close to the natural gramicidin A channel.[26]

Although interesting design strategies for the synthesis of artificial nanotubes and nanochannels exist, still various challenges to the design of discrete nanoobjects remain open.[27] For example, the stability of such nanotubes both in solution and in the solid state is an important issue. In addition, the control over the length of such nanochannels has not been achieved yet without the use of an external constraint, such as for example the use of a lipid bilayer that modulates the in-situ self-assembly of the respective building blocks. Moreover, for potential use of these interesting peptide-based materials in different applications, it would be interesting to develop strategies that allow the dispersion of these materials without the loss over the control of interfacial properties and to tailor the outer diameter of the tube without changing the size of the inner open void.

To address these points, we recently introduced the design concept of modifying self-assembled peptide nanotubes with a synthetic polymeric shell.[28] Using functional polymers, one may think of tailoring interfacial properties in a similar manner as the group of Ghadiri has shown for the precise modulation of the primary sequence of the cyclic peptides. In addition, attaching soft polymers to the surface of peptide nanotubes may also allow for distinct dispersion of single peptide nanotubes. Finally, tailoring the molecular characteristics of the attached polymer molecules affects the overall resulting structure, in particular, it influences the outer diameter, and viscoelastic properties of the surface may be tailored by interaction of the polymers with appropriate solvents.

We reported the synthesis of a cyclic D-/L-peptide that carries functional groups in distinct side chains, which can be used to initiate an atomic transfer polymerization (ATRP). The so-prepared cyclic peptide initiators (CP-ini) self-assemble into peptide nanotubes, with all initiation sites exposed at the outer surface and leaving a inner hollow core, and the internal structure resembles that of an extended β-sheet.[28] In addition, we introduced a first concept of wrapping these CP-ini nanotubes in a covalently bound soft polymeric shell by in-situ surface-induced ATRP of *N*-isopropylacrylamide (NIPAM) in aqueous dispersion.

In this paper, we investigate the surface-initiated ATRP of NIPAM in 2-propanol dispersion, with emphasis on studying the polymerization kinetics and investigating the impact of molecular characteristics, such as the amount of grafted polymer, on the structural characteristics of the resulting PPNT. Using atomic force microscopy (AFM), the thickness (i.e., diameter) and the length of these hybrid nanoobjects are investigated under dry (solvent-free) conditions.

Experimental Section

Materials and Peptide Synthesis. All solvents and reagents were purchased from Sigma and used as received (p.a. grade or higher), if not otherwise stated. DMF was refluxed over ninhydrin to remove any traces of amines and distilled prior to use. 9-Fluorenylmethyloxycarbonyl (Fmoc) protected amino acids, coupling reagents (1-hydroxybenzotriazole (HOBT), 2-(1*H*-benzotriazol-1-yl)-1,1,3,3-tetramethyluronium hexafluorophosphate (HBTU), and (dimethylamino)pyridine (DMAP)), and Wang-Tentagel resin (load: 0.22 mmol/g, Iris Biotech) were used as received. Tris[2-(dimethylamino)ethyl]amine (Me_6TREN) was synthesized and purified according to protocols in the literature.[29] NIPAM monomer (Sigma) was recrystallized from hexane and stored at −20 °C until used.

Synthesis of Model Initiator: 2-Bromo-*N*-butyl-2-methylpropanamide. The model initiator 2-bromo-*N*-butyl-2-methylpropanamide was synthesized by an amidation reaction of butylamine with α-bromoisobutyl bromide. Pyridine (10.6 g, 0.134 mol) and butylamine (11.0 g, 0.160 mol) were dissolved in 20 mL of dichloromethane, and the solution was added dropwise to a solution of α-bromoisobutyl bromide (31.0 g, 0.134 mol) in 50 mL of dichloromethane at 5 °C. The reaction was allowed to warm to room temperature and stirred for 6 h. The solution was concentrated by removing about 80% of the solvent and extracted three times with 100 mL of 2 N HCl and water. After removal of the solvent and drying in a vacuum, a yellow oil was received in 90% yield.

^{1}H NMR ($CDCl_3$, δ in ppm): 3.20 (m, 2H, $-CH_2-NH$), 1.90 (s, 6H, $-CH_3$), 1.50 (m, 2H, $-CH_2$), 1.37 (m, 2H, $-CH_2$), 0.92 (s, 3H, $-CH_3$). ^{13}C NMR ($CDCl_3$, δ in ppm): 170.4 (C═O), 51.1 ($C(CH_3)_2Br$), 39.2 (CH2−NH), 34.2 ($C(CH_3)_2Br$), 32.9 (CH_2) 18.9 (CH_2), 13.5 (CH_3). FTIR (cm^{-1}): υ(amide A): 3350, υ(amide I): 1655, υ(amide II): 1531.

Peptide Synthesis and Self-Assembly. The peptide synthesis, purification, and characterization were reported elsewhere.[28] In brief, the cyclic peptide was prepared using standard solid-phase synthesis protocols. A linear precursor peptide (-L-Asp(OAll)-(D-Ala-L-Lys(Mtt))$_3$-D-Ala-Fmoc) was synthesized on a Tentagel resin using conventional Fmoc chemistry. Cyclization was carried out on resin, and the ATRP initiator 2-bromo-2-methylpropionic acid was subsequently attached to the amine functions at the lysine side chains. The cyclic peptide was cleaved off the resin and purified as previously described.[28]

Self-assembly of the cyclic peptides was carried out according to protocols in the literature.[30] In brief, the cyclic peptide was dissolved in neat TFA in a small vial, and the vial was floated on water in a closed environment. After 3 days, peptide nanotubes were collected by centrifugation, washed neutral with water, and lyophilized. Characterization of the so-prepared peptide initiator (CP-ini) nanotubes with respect to internal structure and morphology was reported elsewhere.[28]

Surface-Initiated Polymerizations. Surface-initiated ATRP reactions were carried out in 2-propanol using CP-ini nanotubes and added sacrificial initiator. Oxygen traces were removed from 2-propanol solution by repeated freeze−thaw cycles under reduced pressure prior to the reactions. NIPAM monomer (4.4 g, 39 mmol) was dissolved in an oxygen-free solution of 2-propanol (40 mL) containing the dispersed CP-ini nanotubes (20 mg, 0.018 mmol) and the model-initiator (62 mg, 0.30 mmol) under an inert-gas atmosphere. The mixture was stirred for 10 min while constantly bubbling nitrogen through the solution. To allow the buildup of the complex between the metal and its ligand, an oxygen-free solution of 2-propanol (10 mL) containing CuBr (30 mg, 0.21 mmol), $CuBr_2$ (10 mg, 0.04 mmol), and Me_6TREN (170 mg, 0.75 mmol) was prepared separately. This solution was then added to the reaction mixture containing peptide-tethered, and free initiator, as well as NIPAM monomer. The latter point was defined as the onset of the polymerization at room temperature, i.e., $t = 0$ min.

Aliquots (10 mL) were taken from the polymerization reaction at regular time intervals. The reaction was stopped by dilution of the aliquots with Cu^{II} dissolved in isPrOH to displace the equilibrium between inactive and active species toward the dormant species. The dispersed peptide−polymer nanotubes were collected by centrifugation, washed repeatedly with 2-propanol, and finally dried in a vacuum. For further analysis, the PPNTs were redispersed in 2-propanol at a concentration of 1 mg/mL.

The supernatant containing free PNIPAM polymer, NIPAM monomer, and the reaction catalyst was passed through a silica gel column to remove the catalyst. Then the solution containing the free PNIPAM and the NIPAM monomer was divided into two vials. One vial was directly used for molar mass analysis of the free polymer by gel permeation chromatography (GPC). The other vial was transferred to a round-bottom flask, and the NIPAM monomer and isPrOH were distilled off (60 °C at 5×10^{-3} mbar) overnight.

Scheme 1. Schematic Description of the Initiator-Modified Cyclic D-/L-Peptide (Left), Self-Assembly of the Peptide into Peptide Nanotubes That Expose the Initiation Moieties at the Outer Surface (Middle), and Surface-Initiated Atom Transfer Polymerization (ATRP) Reaction That Wraps the Peptide Nanotube in Situ in a Soft Polymeric Shell, Thereby Forming a So-Called Peptide−Polymer Nanotube (PPNT, Right)

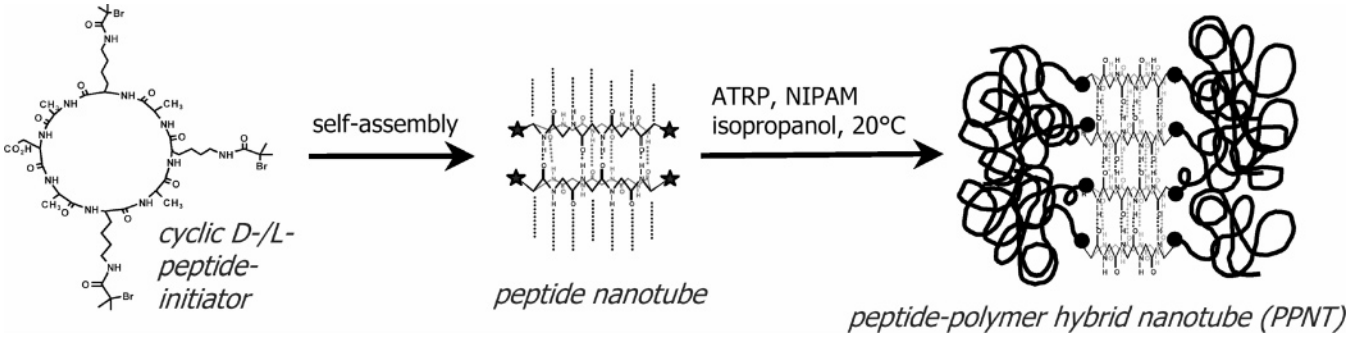

The monomer conversion was determined by gravimetric analysis of the dried polymer.

The number-average molar mass and the polydispersity (PDI = M_w/M_n) were determined by GPC on a Hewlett-Packard Agilent 1100 series using a refractive index detector at $T = 20$ °C. Three columns (PSS GRAM gel, 10^4, 10^3, 30 Å; Polymer Standard Service) in series were used. THF containing 0.1% (v/v) toluene was used as mobile phase (flow rate: 1 mL/min), and the system was calibrated with narrow-disperse poly(methyl methacrylate) (PMMA) standards.

Characterization of PNIPAM−Peptide−Polymer Nanotubes (PNIPAM−PPNT). Characterization of the structure of dried PNIPAM−PPNT was carried out by AFM, using a controller from Digital Instrument series Nanoscope IIIa. Samples were prepared on silicon wafers by drop casting of dispersed nanotubes (1 mg/mL), and the samples were dried in a vacuum prior to the measurements.

FTIR spectra were measured on a BioRad Excalibur series FTS 3000. PPNTs (1 mg/mL in 2-propanol) were drop-casted onto a both-sides polished silicon wafer and dried in a stream of nitrogen prior to the measurements.

Results and Discussion

In a recent work, Stöver and co-workers showed that ATRP of NIPAM in different alcohols, including 2-propanol, can be carried out with sufficient control over reaction conversion and molar mass.[31] As the CP-ini nanotubes are stable in 2-propanol, we applied the same conditions onto the surface-initiated ATRP of NIPAM from self-assembled peptide nanotubes (Scheme 1). Polymerizations were carried out by dispersing the CP-ini nanotubes in 2-propanol and adding free "sacrificial initiator". To this, a mixture of the free initiator and CP-ini nanotubes was added to a solution of monomer, 2-propanol, and appropriate polymerization additives (Me_6TREN, CuBr, and $CuBr_2$), and polymerizations were carried out at room temperature. We targeted a degree of polymerization of $N = 90$. NIPAM was used as the monomer because it yields peptide−polymer nanotubes, where the covalently attached macromolecules are nontoxic and do possess interesting physical properties, such as, for example, a lower critical solution temperature (LCST).[32]

Aliquots of the polymerization feed were taken at regular intervals, and the polymerization was stopped by dilution with excess solvent, followed by the addition of $CuCl_2$. Free polymer was separated from peptide-bound polymer by repeated wash and centrifugation cycles. The free polymer is collected, dried, and analyzed with respect to total weight for conversion analysis.

The sacrificial initiator, used in the present experiments, was especially designed to mimic the lysine side-chain modified initiator of the CP-ini. The chemical structure of this model-initiator is shown in Scheme 2. The sacrificial initiator served

Scheme 2. Schematic Description of the Chemical Structure of the Model Initiator, Which Was Designed in Order To Mimic the Initiator-Modified Lysine Side Chains of the Cyclic Peptide Initiator (CP-ini) Nanotube

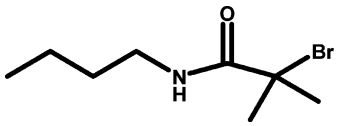

twofold in our investigations. First, the increase in overall concentration of initiation sites in solution is known to suppress early termination reactions at surface-bound growing polymer chains.[33] Second, the PNIPAM polymer formed free in solution can be conveniently separated from the dispersed peptide−polymer nanotubes by simple centrifugation/washing steps, and it can be further analyzed with respect to molar mass. This is in particular important because it is not trivial to directly withdraw information about the molar mass of the individually peptide-linked macromolecules. Using a sacrificial initiator, it was shown that the molar mass of polymers obtained free in solution yield similar masses as compared to surface grafted macromolecules.[34] Thus, in good approximation, surface-confined ATRP kinetics are similar to the kinetics of the same reaction in solution, provided that the chemistries of the initiation sites, monomer, solvent, and polymerization additives are the same as well as viscosities are not too high. Hence, one can obtain molecular characteristics of the surface (i.e., peptide)-attached PNIPAM by analysis of the free polymer formed in solution.

Figure 1a shows the reaction conversion calculated from gravimetric analysis of the free PNIPAM polymer as a function of time. The conversion increases with time, and it can be seen that it levels off at about 35%. If the number of active sites is constant over time, the reaction kinetics in ATRP are expected to follow a first-order behavior (eq 1).[33]

$$\frac{[M_0]}{[M_t]} = \exp(k_p[\sim R^\bullet]t) \qquad (1)$$

Here $[M_t]$ and $[M_0]$ are the monomer concentrations at time t and time $t = 0$, respectively, and $[\sim R^\bullet]$ is the concentration of active sites. Plotting $\ln[M_0]/[M_t]$ against the polymerization time t should therefore yield a linear dependency of the data, with $k_{app} = k_p[\sim R^\bullet]$ (apparent propagation constant) being the slope of the curve. Figure 1b depicts the first-order kinetic plot of the reaction. The data are not linear in time but exhibit a slight downward curved behavior, corresponding to a decrease in the polymerization rate. This decrease is indicative of a loss in active sites and/or an increase of deactivator concentration according

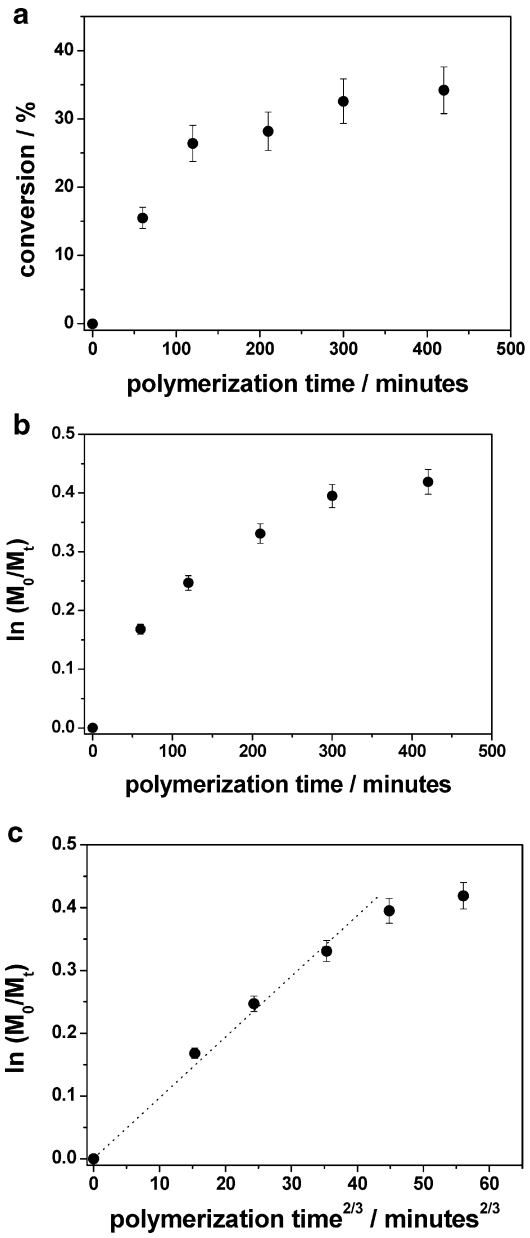

Figure 1. (a) Reaction conversion as a function of polymerization time calculated from monomer consumption, which was measured by gravimetric analysis the free polymer formed during polymerization of *N*-isopropylacrylamide (NIPAM) in 2-propanol using the sacrificial model initiator. Details for the polymerization can be found in the text. (b) Monomer consumption $\ln([M_0]/[M_t])$ of the same reaction as a function of polymerization time t. (c) Monomer consumption $\ln([M_0]/[M_t])$ of the same reaction as a function of $t^{2/3}$. (The dotted line is a guide to the eye.)

to the persistent radical effect.[35] The latter describes how termination by radical recombination leads to an increase of deactivator concentration, which shifts the equilibrium between the active and the inactivated species toward the dormant (i.e., inactive) species. As a result, the monomer consumption should yield a linear dependency of $\ln([M_0]/[M_t])$ against $t^{2/3}$ (eq 2).[35]

$$\frac{[M_0]}{[M_t]} = \exp\left(\frac{3}{2}k_p\left(\frac{K[I]_0}{3k_t}\right)t^{2/3}\right) \qquad (2)$$

Here, k_t is the rate constant of bimolecular termination, $[I]_0$ is the initial concentration of the radical precursor (i.e., initiation sites), and K is the equilibrium constant of activation and deactivation of the latter, respectively.[35]

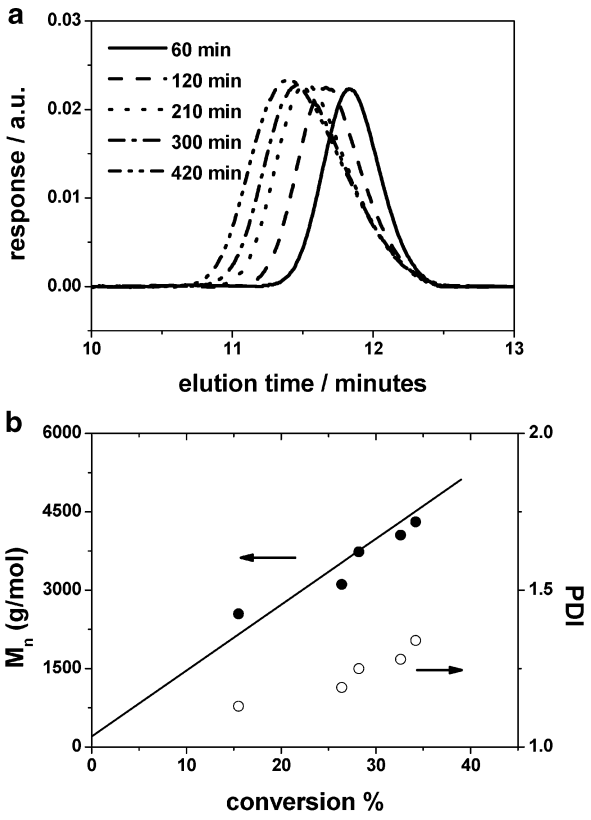

Figure 2. (a) Gel permeation chromatography (GPC) elution traces of linear poly(*N*-isopropylacrylamide) (PNIPAM) obtained from polymerization of *N*-isopropylacrylamide (NIPAM) in 2-propanol using the added sacrificial initiator. (b) Number-average molar mass (M_n) and polydispersity (PDI = M_w/M_n) of the linear PNIPAM as a function of reaction conversion calculated from the GPC measurements using poly(methyl methacrylate) (PMMA) standards.

An almost linear dependency up to 5 h polymerization time is observed, if $\ln[M_0]/[M_t]$ is plotted vs $t^{2/3}$ (Figure 1c). For longer polymerization times, the kinetics still show a slight downward bending with $t^{2/3}$. This can be attributed to a loss in reactive sites, which among other reactions can be due to intramolecular nucleophilic substitution reactions at the reactive end.[36] The latter, again, resembles a termination step within the ATRP kinetics.

The free polymer was further characterized with respect to molar mass and molar mass distribution using GPC measurements with THF as the eluent. Figure 2a shows GPC elution traces for different polymerization times denoted in the figure. With increasing polymerization time the elution curves shift to lower retention times, indicating an increase in the apparent molar mass of the respective polymers.

The number-average molar mass (M_n) of the free polymer and the polydispersity (PDI = M_w/M_n, with M_w being the weight-average molar mass of the polymer) are shown in Figure 2b as a function of reaction conversion. In addition, the theoretically expected molar mass can be calculated according to eq 3.[33]

$$M_n = NM_{mon} = \frac{[M_0]}{[I_0]}pM_{mon} \qquad (3)$$

Here, N is the degree of polymerization, M_{mon} is the molar mass per repeat unit, p is the reaction conversion, and $[M_0]$ and $[I_0]$ are the initial concentrations of monomer and initiator in the polymerization feed, respectively.

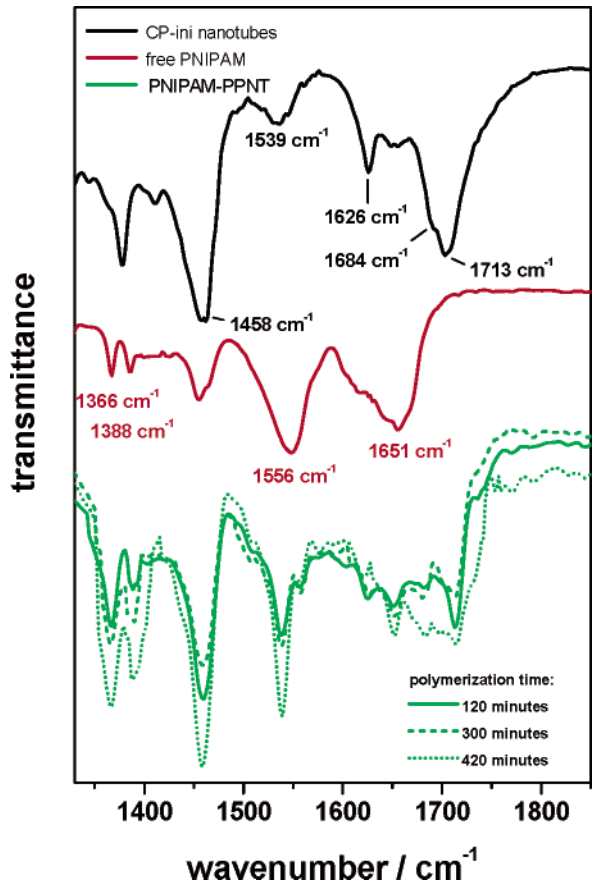

Figure 3. FTIR transmission detail spectra of CP-ini nanotubes (black line), PNIPAM (red line), and PNIPAM−PPNTs (green lines) obtained at different polymerization times (denoted in the figure). Samples were prepared by drop-casting a 2-propanol dispersion/solution onto both-sides polished silicon wafers, drying of the films, and measuring the transmittance in transmission against a nonmodified silicon wafer as background. The preparation of the PNIPAM−PPNT is described in detail in the text.

Figure 2b shows a linear increase of the molar mass of the free PNIPAM as a function of reaction conversion. This is indicative to the controlled "living" nature of the reaction. In addition, the experimentally derived molar mass is similar to the expected molar mass calculated from eq 3 (superimposed to the data as solid line). The latter finding suggests that there are no termination reactions present, a finding that contrasts the above measured kinetics, however. A possible reason for this could be an overestimation of the molar mass of the PNIPAM by GPC analysis due to self-aggregation and/or the use of a nonappropriate standard in the GPC analytics. An overestimation of the molar mass would apply for all samples, and the linear increase of the mass with polymerization time still holds, indicating good reproducibility of the experiment. The polydispersity shows a slight increase from 1.2 at 15% conversion to 1.4 at about 35% conversion. This can be attributed to termination reactions as well as other side reactions. The polydispersities are all well below typical values obtained through conventional radical polymerizations.[33]

To analyze the chemical identity, PNIPAM−PPNT were characterized using FTIR. To this, a solution containing dispersed PPNT was drop-casted onto a silicon wafer, dried, and measured in transmission against a nonmodified silicon wafer as the background. Figure 3 shows FTIR detail spectra (green lines) of three examples of PNIPAM−PPNT obtained at three different polymerization times (denoted in the figure). In addition, the spectra of the nonmodified CP-ini nanotube (black line) and linear PNIPAM (red line) are superimposed to the data. With the CP-ini nanotube distinct peaks at 1458 cm^{-1} (bending deformation; −C−H), 1539 cm^{-1} (amide II), 1626 cm^{-1} (amide I), 1684 cm^{-1} (amide I), and 1713 cm^{-1} (C═O, carboxylic acid) are observed that can be attributed to vibrational modes of the peptide nanotube. In particular, the peaks at 1626 and 1684 cm^{-1} are indicative to the internal β-sheet assembly of the nanotube.[37] PNIPAM (red) exhibits peaks at 1366 cm^{-1} ($-CH_3$), 1388 cm^{-1} ($-CH_3$), 1458 cm^{-1} (C−H), 1556 cm^{-1} (amide II), and 1651 cm^{-1} (amide I). The peaks at 1366 and 1388 cm^{-1} correspond to vibrational modes of the two methyl groups in the PNIPAM side chain. The peak at 1458 cm^{-1} corresponds to the bending deformation of the backbone −CH groups. The peaks at 1539 cm^{-1} (−N−H deformation in the side-chain amide group) and 1651 cm^{-1} (amide I) correspond to the amide groups in the PNIPAM side chain and indicate a random structure of the latter.

The detailed spectra of the PNIPAM−PPNT (green lines) resemble a superposition of the respective bulk spectra, showing all peaks discussed before. This can be taken as a direct proof of the chemical identity of the hybrid material. With increasing polymerization time, in principle, one would expect an increase of the PNIPAM signals relative to the CP nanotube signals. The PNIPAM−PPNT exhibit a rather complex spectrum in the amide I and amide II region; therefore, it is not trivial to analyze the spectra in a very quantitative way. We normalized the spectra with respect to the same peak intensity of the amide I (1626 cm^{-1}) peak of the peptide. Qualitatively, the integral intensities of the peaks at 1366 and 1388 cm^{-1}, which correspond to vibrational modes of the two methyl groups in the PNIPAM side chain, increase with increasing polymerization time. However, also the peak at 1556 cm^{-1} increases at the same time. Quantitative information about the increase in the amount of grafted polymer with increasing polymerization time can be withdrawn from further analysis of the dry PPNT structure, i.e., the dry nanotube diameter.

To study the structure and morphology of the prepared PPNT, we used atomic force microscopy (AFM) in tapping mode. PNIPAM−PPNT's were adsorbed by drop-casting from dilute 2-propanol dispersion onto a silicon wafer followed by drying of the samples in a vacuum. The AFM was shown to be a powerful method providing valuable and accurate information about the shape, size, and molar mass of polymer colloids adsorbed to solid surfaces.[38] In particular, single macromolecules of complex architecture such as cylindrical brushes, dendrimers, and worm-, star-, and rodlike objects were analyzed with respect to the height and length distribution with sub-nanometer precission.[39]

Figure 4a shows an AFM height image of CP-ini nanotubes (left) as well as AFM height (middle) and phase (right) micrographs of PNIPAM-PPNT's adsorbed to a silicon wafer. The CP-ini nanotubes tend to aggregate on the surface in 2-dimensional fiberlike structures, whereas after polymerization single dispersed nanotubes were visible at the surface. We recently reported cross-sectional analysis of the CP-ini nanotubes, showing that the fibers originate from sweeping rodlike objects together on the surface by capillary forces rather than the fibers formed in solution.[28]

Figure 4b depicts AFM height (left) and phase (right) micrographs of a PNIPAM−PPNT single nanotube. The PPNT resembles the structure of a rigid rodlike nanoobject. In Figure 4c, the cross-section analysis of the same PPNT (blue line) is shown together with a cross-section analysis of a CP-ini

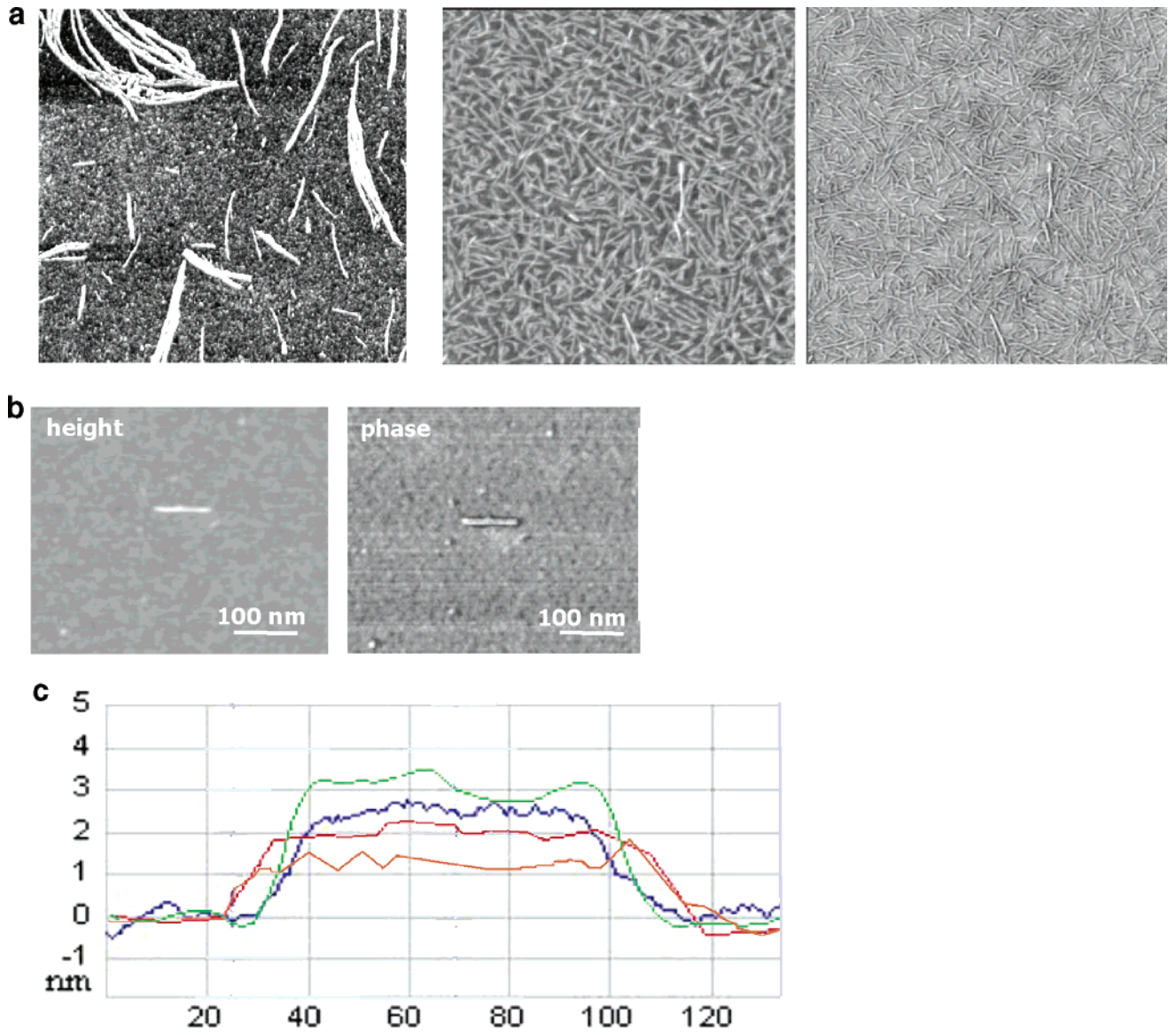

Figure 4. (a) Atomic force microscopy (AFM) height image (left, lateral scale: 2 μm; *z*-scale: 0−5 nm) of CP-ini nanotubes adsorbed on a silicon wafer and AFM height image (middle, lateral scale: 2 μm; *z*-scale: 0−15 nm) and phase micrograph (right, lateral scale: 2 μm) of PNIPAM−PPNTs adsorbed to a silicon wafer from 2-propanol dispersion (polymerization time in this sample: 60 min). (b) AFM height micrograph (left, lateral scale: 0.5 μm; *z*-scale: 0−10 nm) and phase micrograph (right, lateral scale: 0.5 μm) of a dried PNIPAM−PPNT single nanotube. (c) Cross-section analysis of the same PPNT as shown in (b) (blue line). Superimposed to this cross section are further cross sections of a CP-ini nanotube (no polymer shell, i.e., polymerization time: 0 min, orange line) and cross sections of single PPNT's after 60 min (red line) and 300 min polymerization time (green line).

nanotube (i.e., no polymer attached, orange line) and a PNIPAM−PPNT obtained after 60 min (red) and 300 min (green) polymerization time, respectively. After polymerization, a thin polymer film covers the respective peptide nanotube core in a very homogeneous manner and with very low roughness along the tube's surface (long axis). Even small changes in the absolute (dry) height of a few angstroms can be easily visualized by AFM. Hence, by statistical analysis of the cross sections of single PPNT's, one is capable of calculating mean average values for the structural characteristics in dry conditions.

An ensemble of 200 PPNT's was characterized using AFM cross-section analysis of surface-adsorbed, dry PPNT's with respect to their height and length. Figure 5a shows examples of height distributions at different polymerization times (given in the figure). The distribution of the CP-ini nanotubes carrying no polymer (i.e., at polymerization time $t = 0$ min) is very narrow, and the mean average height is about 1.7 ± 0.1 nm.[28] With increasing polymerization time, the mean average value of the height increases to about 3.5 ± 0.3 nm after 420 min polymerization time.

The cross section of the PPNT along the short axis resembles that of either a cylinder or an ellipse, as schematically outlined in Scheme 3. The latter strongly depends on the interaction of the grafted polymer chains with the underlying surface as well as on the length of the chains. For long and adsorbing chains, an ellipse-like structure may be expected, whereas nonadsorbing (and/or short) chains presumably render the structure cylinder-like. The AFM tip itself can cause a deformation of soft nanoobjects during visualization. This source of flattening cannot inherently be eliminated but can be controlled by applying identical force between the AFM tip and the substrate during imaging of all samples of comparison.

Because we grafted rather short chains onto the CP-ini nanotube core, in good approximation, we can treat the PPNT to be cylinder-like in structure. The overall volume of the PPNT

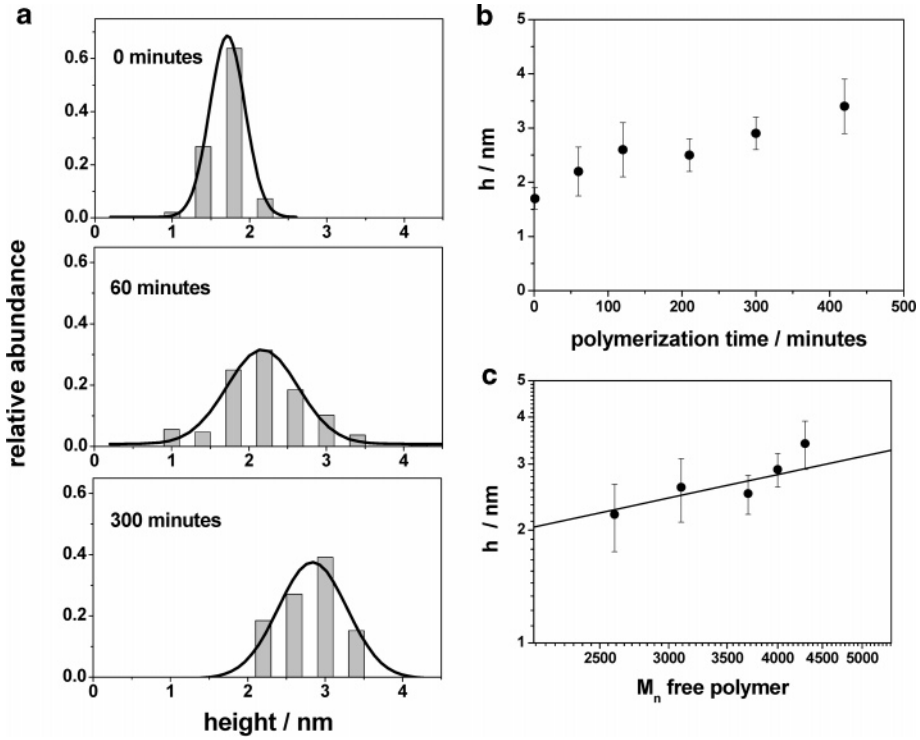

Figure 5. (a) Relative abundance of the dry height of CP-ini nanotube and PNIPAM−PPNT determined by statistical cross-section analysis. Gaussian fits to the distributions are shown as solid lines. Different polymerization times are given in the figure. (b) Dry height h of the PNIPAM−PPNT as a function of polymerization time. (c) Dry height h of the PNIPAM−PPNT's as a function of the number-average molar mass of the free polymer, obtained from using sacrificial initiator during surface-induced polymerizations. The solid line represents a linear function of the height vs molar mass (M_n) having a constant slope of $m = 0.5$.

Scheme 3. Schematic Description of Possible Geometrical Structures of Dried Peptide−Polymer Nanotubes Adsorbed to a Solid Surface[a]

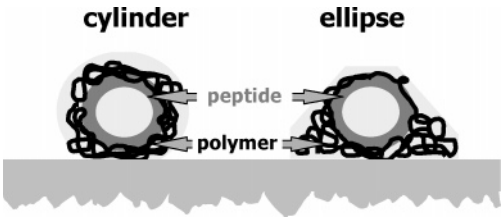

[a] Depending of the length of the polymer arms as well as on the polymer−surface interactions, either a cylinder-like morphology can be anticipated, where the chains are collapsed onto the peptide nanotubes core, or a more ellipse-like morphology is expected, where individual chains are adsorbing in a flat conformation.

is then given by the volume of the internal peptide nanotube and the polymer volume: $V_{PPNT} = V_{CP-ini} + V_{PNIPAM}$. The volume of the grafted PNIPAM is given by the molar mass and the number of the attached polymer chains as well as the density of the polymer. Assuming a cylindrical geometry, the solvent free height of the PPNT cylinder can be theroetically calculated according to eq 4.

$$h_{PPNT} = h_{CP-ini} + \sqrt{\frac{M_n n}{\rho_{PNIPAM}} \frac{4}{\pi l_{PPNT}}} = h_{CP-ini} + \text{const}\sqrt{M_n} \quad (4)$$

Here, h_{CP-ini} is the height of the CP-ini nanotube, h_{PPNT} is the solvent-free height, l_{PPNT} is the length of the peptide−polymer nanotube, n is the number of grafted chains per length, and ρ is the density of the polymer. Assuming that the number of grafted chains and the length of the PPNT do not change with increasing polymerization time, the height should increase with $M_n^{0.5}$. Figure 5c shows the height of the PPNT as a function of the molar mass of the free polymer. The solid line represents a linear function of the height with the polymerization time having a constant slope of 0.5. Thus, it represents an increase of the height of an equivalent cylinder with its mass, provided that the length of the cylinder stays constant. The experimental data can be sufficiently described by the theoretical increase of the height of this equivalent cylinder. This indicates that, by adjusting the molar mass of the attached polymer chains, one can reproducibly control the dry height of the peptide−polymer nanotubes, i.e., the outer diameter of the PPNT.

Besides the molar mass, it is the grafting density, i.e., the number of polymer chains attached to each peptide nanotube, that influences the overall polymer amount and therefore the solvent-free height. Assuming that the polymerization kinetics at the surface of the dispersed peptide nanotubes is similar to the kinetics in solution, the average molar mass obtained from free (sacrificial) initiator is similar to the molar mass of the peptide-attached macromolecules. Again, using the cylinder model to describe the dry structure of the PPNT, one can calculate the theoretical volume and thus the theoretical height h_{th} of an equivalent cylinder (eq 5).

$$h_{th} = h_{CP-ini} + \sqrt{\frac{M_n n_{th}}{\rho_{PNIPAM}} \frac{4}{\pi l_{PPNT}}} = h_{CP-ini} + \text{const}\sqrt{n_{th}} \quad (5)$$

Here n_{th} is the number of grafted chains per peptide−polymer nanotube (i.e., $n_{th} = 3$ at 100% initiator efficiency). Comparing the height at quantitative conversion (h_{th}) with the experimentally measured height of the dry PPNT, one can calculate the relative amount of grafted chains, corresponding to an apparent

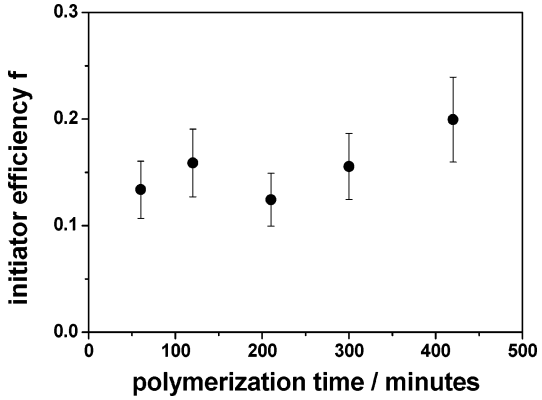

Figure 6. Apparent initiation efficiency *f* of the peptide nanotube-bound initiators as a function of polymerization time. The efficiency was calculated according to eqs 5 and 6.

initiation efficiency *f* of the peptide-attached initiators (eq 6).

$$\frac{h^2_{\mathrm{PPNT}}}{h^2_{\mathrm{th}}} = \frac{n_{\mathrm{th}}}{n_{\mathrm{PPNT}}} = f \tag{6}$$

Figure 6 shows the apparent initiation efficiency, *f*, calculated from eqs 5 and 6 as a function of the polymerization time. With increasing polymerization time, the number of grafted polymer chains does not significantly vary; thus, it stays constant at about 15%. From a first point of view this number sounds rather small. However, there are possible reasons for this. First, taking into account the high grafting density of the initiation sites on the surface of the peptide nanotube, one may expect a sterical hindrance of the interaction of the copper−ligand complex with individual initiation sites at a time. The typical ring−ring distance is about 0.5 nm,[22] and as every ring carries three initiation sites, the average distance of initiator functions on the surface of the nanotube can be estimated to be about 1 nm. This kinetic limitation becomes even more prominent, once a single growing chain at the surface possibly covers neighboring "inactive" sites. Another possible source for a low graft density may be early termination reactions with the amide-functional initiation sites. A third reason may originate from possible overestimation of the molar mass of the linear PNIPAM by GPC analysis. In this case, the theoretical height will be overestimated, too; thus, eqs 5 and 6 yield lower values for the apparent initiation efficiency.

Besides the height (i.e., outer diameter), there is the length of artificial nanotubes that is of interest for prospective applications of these novel hybrid materials. With increasing polymerization time, the length distributions, analyzed by AFM, do not change significantly (Figure 7a). Only one-dimensional objects with lengths well above 50 nm were accessed for length analysis. Smaller objects increasingly present at the surface at higher polymerization times were not taken into account but analyzed separately (see below). The distributions shown here were analyzed with respect to the number-average (L_n) and weight-average (L_w) length. Both parameters are defined by eqs 7 and 8:

$$L_{\mathrm{n}} = \sum_i \frac{n_i L_i}{n_i} \tag{7}$$

$$L_{\mathrm{w}} = \sum_i \frac{n_i L_i^{\,2}}{n_i L_i} \tag{8}$$

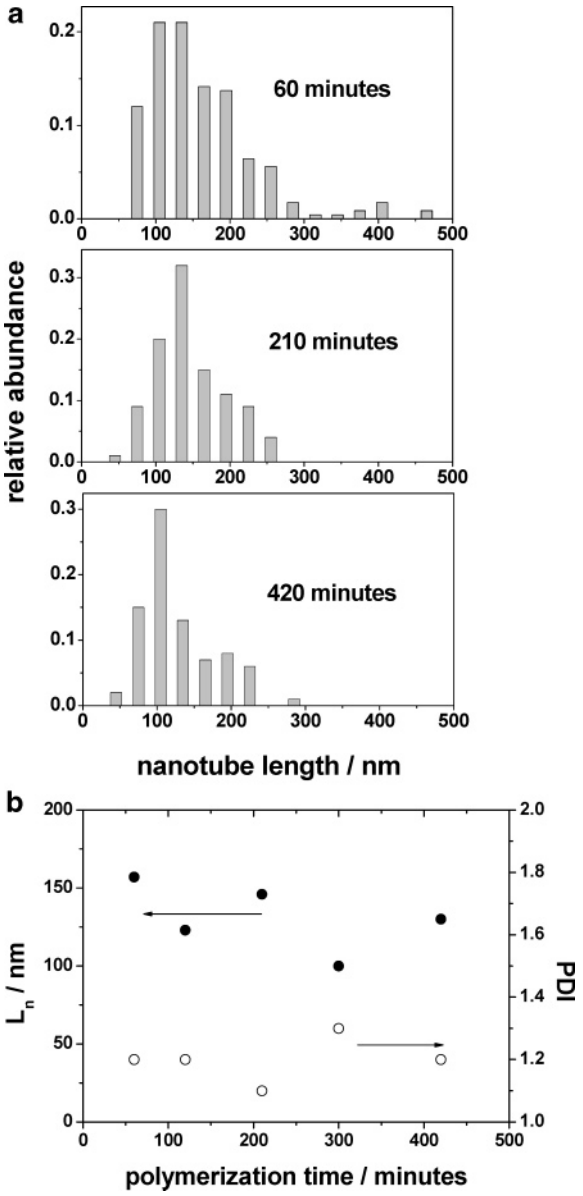

Figure 7. (a) Relative abundance of the length of dry PNIPAM−PPNT calculated from statistical cross-section analysis of atomic force microscopy (AFM) height images. Different polymerization times are denoted in the figure. (b) Number-average length L_n as well as polydispersity (PDI = L_w/L_n) of the PNIPAM−PPNT as a function of polymerization time. Both parameters were calculated using eqs 7 and 8.

Accordingly, the polydispersity (PDI) is defined as PDI = L_w/L_n. Figure 7b shows the number-average length of the PPNT together with the corresponding PDI's as a function of the polymerization time. The length stays more or less constant with increasing polymerization time around 120 nm, and the PDI is in all cases about 1.2. We recently showed that the length of the CP-ini nanotubes (i.e., no polymer attached) is not trivial to analyze with respect to length distribution due to the fact that these nanotubes tend to form larger nonspecific aggregates.[28] The shortest lengths reported with CP-ini nanotube objects are about 100−500 nm.[28]

Besides an increase in height and an almost constant length of the PPNT, an interesting observation was made with increasing polymerization time. First the absolute concentration of PPNT decreases, and second, smaller objects of uniform size appear. The latter becomes very prominent at polymerization times on or above 5 h.

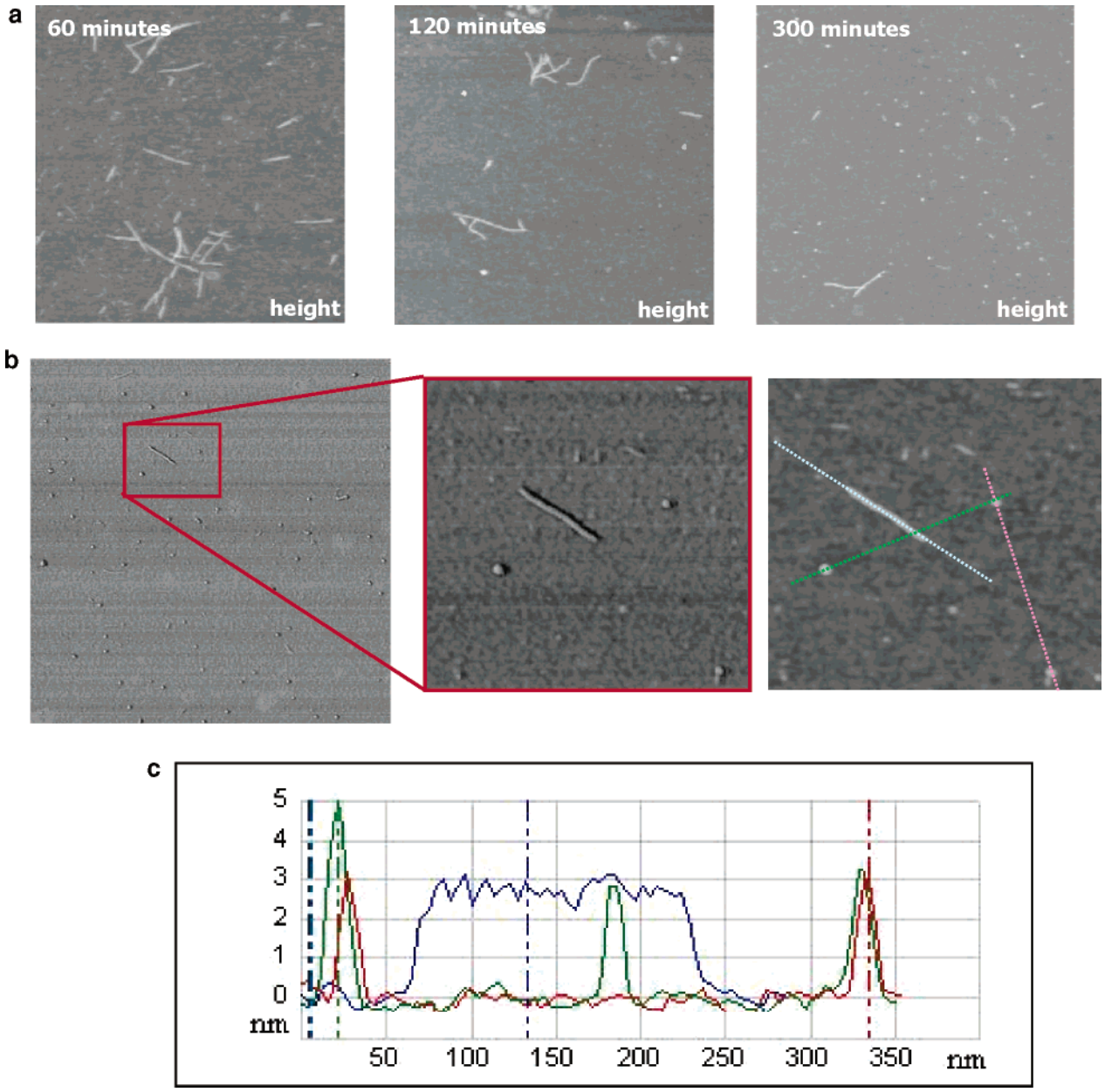

Figure 8. (a) Atomic force microscopy (AFM) height images (lateral scale: 1 μm, *z*-scale: 0−10 nm) of dry PNIPAM−PPNT adsorbed to a silicon wafer. Different polymerization times are given as insets in the images. (b) AFM phase image (left, lateral scale: 2 μm), zoom-in (middle, lateral scale: 0.7 μm), and AFM height micrograph (right, lateral scale: 0.7 μm, *z*-scale: 0−10 nm) of dry PNIPAM−PPNT adsorbed to a silicon wafer. (c) Cross-section analysis along the three artificial lines superimposed to the AFM height image shown in (b).

Figure 8a shows examples of AFM height micrographs of adsorbed PNIPAM-PPNT's obtained at three different polymerization times (denoted in the figure). In all cases individual PPNT's can be visualized and analyzed with respect to height and length. The number of visualized PPNT's is decreasing with increasing polymerization time. Above 5 h of polymerization time small uniform particles are increasingly present at the surface. Note that all PNIPAM−PPNT's have been drop-casted in these experiments at identical concentrations.

Figure 8b shows two AFM phase micrograph and one AFM height micrograph (polymerization time: 420 min). In the large-scale phase image (left), a large number of small particles are visible next to an intact single PPNT. As is evident from a zoom-in region of the phase image (middle), these particles possess a core−shell type morphology, indicated by the black halo surrounding the brighter core. This morphology is similar to the one observed with the peptide−polymer nanotube itself. A cross-section analysis along the three differently colored artificial lines drawn into the height image was performed. Figure 8b shows the cross sections (same colors used as in height image). The height of the smaller objects is in this sample similar to the height of the single PPNT. We analyzed more samples in order to compare the dry heights of the smaller objects with that of the PPNT. Figure 9 shows the dry particle height (open symbols) as well as the dry hybrid nanotube height (closed symbols) as a function of polymerization time. At 60 min polymerization time, only intact PPNTs can be detected. Already at 120 min of polymerization time, we observe the appearance of few small particles that were analyzed by AFM cross sections. The number of particles increases with increasing polymerization time, and above 5 h polymerization time there are only few intact PPNT left, whereas AFM height images show a large number of particles. The dry height of the smaller objects is in all samples the same as the height of the PPNT (Figure 9). This

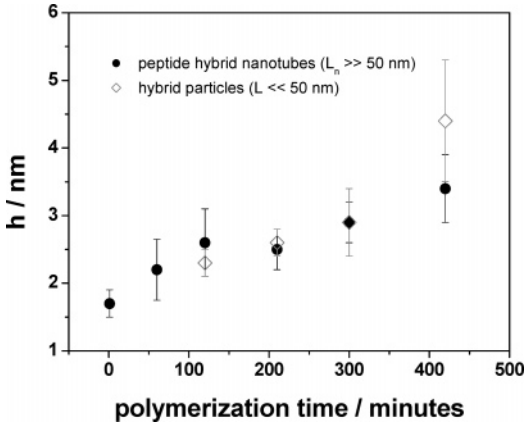

Figure 9. Dry height *h* of PNIPAM−PPNT (closed circles) and of smaller PNIPAM hybrid nanoobjects (open diamonds) as a function of polymerization time. The dry height for both materials was determined by statistical analysis of cross sections of AFM height micrographs. PPNT's obtained at different polymerization times were adsorbed to a silicon wafer, dried, and analyzed in tapping mode under identical conditions. Objects much larger than 50 nm in length (L_n) were assigned as "nanotubes" and accordingly analyzed separately from objects smaller than 50 nm in length ("particles").

suggests that the particles arise from peptide−polymer nanotubes, which were broken up into smaller hybrid objects. One can think of possible reasons that can cause the breakup of the nanotubes. First, polymer excluded volume interactions potentially result in repulsive forces between the nanotube anchored chains, which leads to a separation of individual rings, as the latter are hold together only by cooperative weak interactions (H-bonds). Second, the interaction of the surface itself with the nanoobjects may play a role in this phenomenon. It was recently reported that such interactions sometimes generate forces strong enough to break covalent bonds.[40] With respect to the latter, in future work, it is also interesting to question the influence of the drying procedure of the solvent at the surface and, in particular, capillary forces that are exerted during drying of the surfaces.

Conclusions

Peptide−polymer nanotubes (PPNT's) were prepared by self-assembling cyclic peptides that carry ATRP initiators in distinct side chains and wrapping these supramolecular 1-dimensional nanoobjects in a soft polymeric shell by in-situ surface-initiated ATRP of NIPAM in 2-propanol dispersion. The reaction kinetics as well as molar masses were analyzed from free PNIPAM polymer, obtained through adding a "sacrificial initiator" to the surface-initiated polymerizations. $\ln([M_0]/[M_t])$ is not linear in t, but rather follows a $t^{2/3}$ dependency, indicating that with increasing polymerization time there is a loss in active species and/or an increase in deactivator concentration. The molar mass of the PNIPAM increases in a linear fashion with reaction conversion, which indicates that the length of the polymer chains can be controlled by adjusting the appropriate polymerization parameters (i.e., the polymerization time).

The solvent-free height of a surface-adsorbed PPNT, as measured by statistical analysis of cross sections of AFM height micrographs, increases with increasing molar mass of the attached PNIPAM chains. The latter indicates that the size of the soft polymeric shell can be precisely controlled by adjusting the molar mass of the peptide-attached polymer chains. For the first time, the outer diameter of a self-assembled peptide (hybrid) nanotube can be varied without changes to the primary peptide sequence.

The length of the PPNT remains constant with increasing polymerization time; however, at larger polymerization time, a decrease in concentration of the PPNT is observed, and smaller particles are increasingly present. Because of similarities in height and morphology of the particles and the PPNT, the latter finding can be attributed to a breakup of the PPNT into smaller (uniform) nanoobjects. Possible reasons for this may be repulsive forces exerted between the surface-attached polymer chains that eventually overcome the forces that hold individual peptide rings together. Work to test this hypotheses and to explore the extent to which one can make use of this phenomenon to precisely "cut", i.e., downsize, the PPNTs into well-defined small PPNT objects is currently being investigated in the supramolecular synthesis of well-defined hybrid nanotubes.

Acknowledgment. The authors like to acknowledge fruitful interactions, discussions, and collaborations on the AFM analysis of surface-adsorbed peptide−polymer hybrid nanotubes with Dr. Svetlana Santer (Prokhorova) and Alexey Kopychev at the IMTEK. We thank Prof. J. Rühe and Dr. O. Prucker (IMTEK) for valuable support and discussions. Financial support through the Emmy Noether Program of the DFG (Grant BI738/1-3) as well as through the Landesstiftung Baden Württemberg gGmbH and the Fonds der chemischen Industrie is gratefully acknowledged. J.C. thanks the DAAD for a Ph.D. fellowship.

References and Notes

(1) Eisenberg, B. *Acc. Chem. Res.* **1998**, *31*, 117−123.
(2) Alberts, B.; Bray, D.; Lewis, J.; Raff, M.; Roberts, K.; Watson, J. D. *Molecular Biology of the Cell*; Garland Publishing: New York, 1994.
(3) Preston, G. M.; Carrol, P.; Guggino, W. B.; Agre, P. *Science* **1992**, *256*, 385−387.
(4) Dutzler, R.; Campbell, E. B.; Cadene, M.; Chait, B. T.; MacKinnon, R. *Nature (London)* **2002**, *415*, 287−294.
(5) Zwickl, P.; Voges, D.; Baumeister, W. *Philos. Trans. R. Soc. London B* **1999**, *354*, 1501−1511.
(6) Chadwick, D. J., Cardew, D., Eds.; *Gramicidin and Related Ion Channel-Forming Peptides*; John Wiley & Sons Ltd.: London, 1999.
(7) Mitchell, D. T.; Lee, S. B.; Trofin, L.; Li, N.; Nevanen, T. K.; Söderlund, H.; Martin, C. R. *J. Am. Chem. Soc.* **2002**, *124*, 11864−11865.
(8) Karlsson, R.; Karlsson, A.; Orwar, O. *J. Am. Chem. Soc.* **2003**, *125*, 8442−8443.
(9) Percec, V.; Ahn, C. H.; Ungar, G.; Yeardley, D. J. P.; Moller, M.; Sheiko, S. S. *Nature (London)* **1998**, *391*, 161−164.
(10) Das, G.; Talukadar, P.; Matole, S. *Science* **2002**, *298*, 1600−1602.
(11) Fernandez-Lopez, S.; Kim, H. S.; Choi, E. C.; Delagado, M.; Granja, J. R.; Khasanov, A.; Ghadiri, M. R. *Nature (London)* **2001**, *412*, 452−455.
(12) Balbo Block, M. A.; Kaiser, C.; Khan, A.; Hecht, S. *Top. Curr. Chem.* **2005**, *245*, 89−150.
(13) Berl, V.; Huc, I.; Khoury, R. G.; Krische, M. J.; Lehn, J. M. *Nature (London)* **2000**, *407*, 720−723.
(14) Nelson, J. C.; Saven, J. G.; Moore, J. S. *Science* **1997**, *277*, 1793−1796.
(15) Fenniri, H.; Packiarajan, M.; Vidale, K. L.; Sherman, D. M.; Hallenga, K.; Wood, K. V.; Stowell, J. G. *J. Am. Chem. Soc.* **2001**, *123*, 3854−3855.
(16) Sakai, N.; Matile, S. *Chem Commun.* **2003**, *20*, 2514−2523.
(17) Song, L.; Hobaugh, M. R.; Shustak, C.; Cheley, S.; Bailey, S.; Gouaux, J. E. *Science* **1996**, *274*, 1859−1865.
(18) Grave, C.; Schlüter, A. D. *Eur. J. Org. Chem.* **2002**, *18*, 3075−3098.
(19) Venkataraman, D.; Lee, S.; Zhang, J.; Moore, J. S. *Nature (London)* **1994**, *371*, 591−593.
(20) Höger, S.; Morrison, D. L.; Enkelmann, V. *J. Am. Chem. Soc.* **1999**, *124*, 6734−6736.
(21) De Santis, P.; Morosetti, S.; Rizzo, R. *Macromolecules* **1974**, *7*, 52−58.
(22) Ghadiri, M. R.; Granja, J. R.; Milligan, R. A.; McRee, D. E.; Khazanovich, N. *Nature (London)* **1993**, *366*, 324−327.
(23) Hartgerink, J. D.; Granja, J. R.; Milligan, R. A.; Ghadiri, M. R. *J. Am. Chem. Soc.* **1996**, *118*, 43−50.
(24) Ghadiri, M. R. *Adv. Mater.* **1995**, *7*, 675−677.

(25) Ghadiri, M. R.; Kobayashi, K.; Granja, J. R.; Chadha, R. K.; McRee, D. E. *Angew. Chem.* **1995**, *107*, 76−78; *Angew. Chem., Int. Ed. Engl.* **1995**, *34*, 93−95.
(26) Clark, T. D.; Buehler, L. K.; Ghadiri, M. R. *J. Am. Chem. Soc.* **1998**, *120*, 651−656.
(27) Balbo Block, M. A.; Hecht, S. *Angew. Chem., Int. Ed.* **2005**, *44*, 6986−6989.
(28) Couet, J.; Samuel, J. D. J. S.; Kopyshev, A.; Santer, S.; Biesalski, M. *Angew. Chem., Int. Ed.* **2005**, *44*, 3297−3301.
(29) Ciampolini, M.; Nardi, N. *Inorg. Chem.* **1966**, *5*, 41−43.
(30) Bong, D. T.; Clark, T. D.; Granja, J. R.; Ghadiri, M. R. *Angew. Chem., Int. Ed.* **2001**, *40*, 988−1011.
(31) Gil, E. S.; Hudson, S. A. *Prog. Polym. Sci.* **2004**, *29*, 1173−1222.
(32) Xia, Y.; Yin, X.; Burke, N. A. D.; Stöver, H. D. H. *Macromolecules* **2005**, *38*, 5937−5943.
(33) Matyjaszewski, K.; Xia, J. *Chem. Rev.* **2001**, *101*, 2921−2990.
(34) von Werne, T.; Patten, T. E. *J. Am. Chem. Soc.* **2001**, *123*, 7497−7505.
(35) Fischer, H. *Chem. Rev.* **2001**, *101*, 3581−3610.
(36) Teodorescu, M.; Matyjaszewski, K. *Macromolecules* **1999**, *32*, 4826−4831.
(37) Seewald, N.; Jakubke, H. D. *Peptides: Chemistry and Biology*; Wiley-VCH: Weinheim, 2002.
(38) Sheiko, S. S.; Moller, M. *Chem. Rev.* **2001**, *101*, 4099−4123.
(39) Beers, K. L.; Gaynor, S. G.; Matyjaszewski, K.; Sheiko, S. S.; Moller, M. *Macromolecules* **1998**, *31*, 9413−9415.
(40) Sheiko, S. S.; Sun, F. C.; Randall, A.; Shirvanyants, D.; Rubinstein, M.; Lee, H.; Matyjaszewski, K. *Nature (London)* **2006**, *440*, 191−194.

MA061200J